UCRL-JC-135596
PREPRINT

Effect of Controlled Potential on SCC of Nuclear Waste Package Container Materials

A.K. Roy
M.K. Spragge
B.Y. Lum

This paper was prepared for submittal to the
Corrosion/2000 Conference
Orlando, Florida
March 26-31, 2000

August 1, 1999

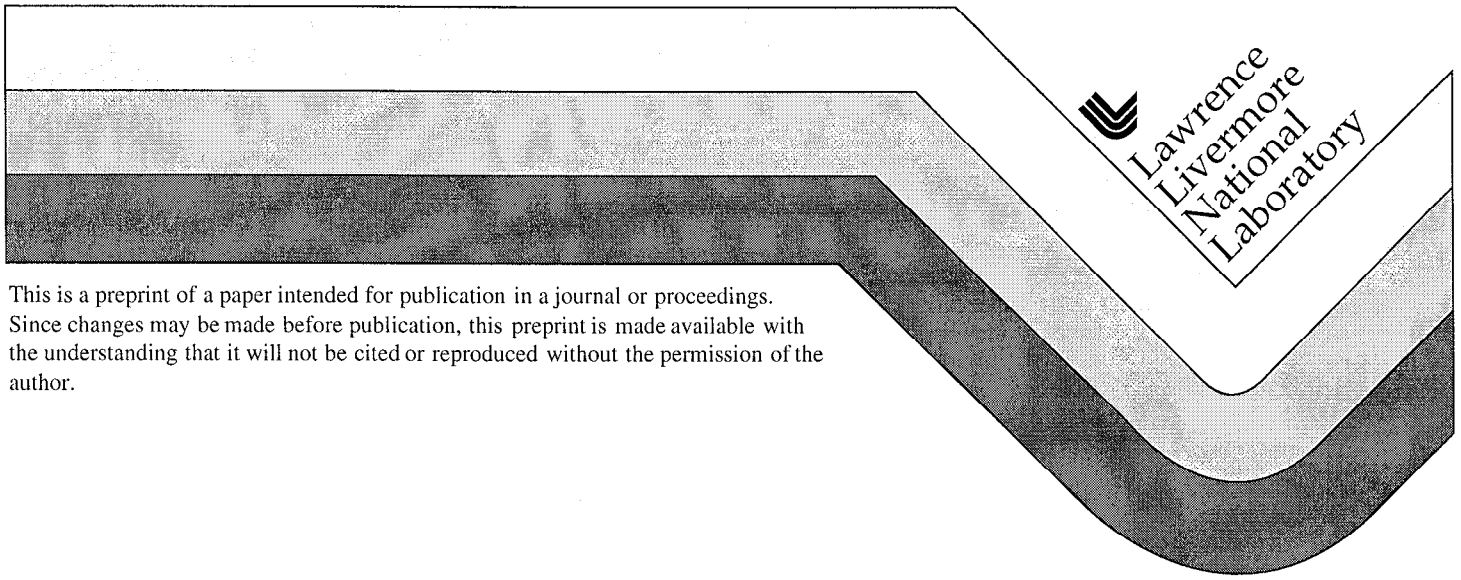

Effect of Controlled Potential on SCC of Nuclear Waste Package Container Materials

Ajit K. Roy
Maura K. Spragge
Beverly Y. Lum

This paper was prepared for submittal to the
Corrosion/2000 Conference
Orlando, Florida
March 26-31, 2000

August 1999

EFFECT OF CONTROLLED POTENTIAL ON SCC OF NUCLEAR WASTE PACKAGE CONTAINER MATERIALS

Ajit K. Roy
Framatome Cogema Fuels
c/o LLNL (On Assignment)
7000 East Ave, M/S L-631
Livermore, CA 94550

Maura K. Spragge
Beverly Y. Lum
Lawrence Livermore National Laboratory
7000 East Ave, M/S L-201
Livermore, CA 94550

ABSTRACT

The slow-strain-rate (SSR) test technique was used to evaluate the susceptibility of Titanium (Ti) Gr-7 (UNS R52400) and Ti Gr-12 (UNS R53400) to stress corrosion cracking (SCC). Ti Gr-7 and Ti Gr-12 are two candidate container materials for the multi-barrier package for nuclear waste. The tests were done in a deaerated 90°C acidic brine (pH ≈ 2.7) containing 5 weight percent (wt%) sodium chloride (NaCl) using a strain rate of 3.3×10^{-6} sec^{-1}. Before being tested in the acidic brine, specimens of each alloy were pulled inside the test chamber in the dry condition at ambient temperature. Then, while in the test solution, specimens were strained under different cathodic (negative) controlled electrochemical potentials. These controlled potentials were selected based on the corrosion potential measured in the test solution before the specimens were strained. Results indicate that the times to failure (TTF) for Ti Gr-12 were much shorter than those for Ti Gr-7. Furthermore, as the applied potential became more cathodic, Ti Gr-12 showed reduced ductility in terms of percent reduction in area (%RA) and true fracture stress (σ_f). In addition, TTF and percent elongation (%El) reached the minimum values when Ti Gr-12 was tested under an impressed potential of –1162 mV. However, for Ti Gr-7, all these ductility parameters were not significantly influenced by the changes in applied potential. In general, the results of hydrogen analysis by secondary ion mass spectrometry (SIMS) showed increased hydrogen concentration at more cathodic controlled potentials. Optical microscopy and scanning electron microscopy (SEM) were used to evaluate the morphology of cracking both at the primary fracture face and the secondary cracks along the gage section of the broken tensile specimen. Transgranular secondary cracks were observed in both alloys possibly resulting from the formation of brittle titanium hydrides due to cathodic charging. The primary fracture face was characterized by dimpled microstructure indicating ductile failure.

Keywords: Stress corrosion cracking, hydrogen embrittlement, titanium alloys, slow-strain-rate test, and controlled electrochemical potential.

INTRODUCTION

The waste package designed for spent nuclear fuel and defense high-level waste during the viability assessment period has focused on all-metallic, multi-barrier concepts to accommodate geologic disposal in the potential repository at Yucca Mountain, near Las Vegas, Nevada. This design incorporates a thick outer corrosion-allowance metal barrier over a thinner inner container made of a suitable corrosion-resistant alloy. The outer barrier is intended to maintain the structural integrity of the waste package and also provide galvanic protection to the inner container from the potential repository environment should the outer container be breached. During the current licensing application period, however, some changes in container materials are being considered. The precise method of fabricating the waste packages is yet to be finalized. Regardless of the fabrication technique, some form of welding of the container's metallic materials will likely be involved in producing cylindrical packages of large diameters. This welding could generate enough residual stresses to cause the waste package materials to become susceptible to SCC as they are placed in the potential repository environment. This paper presents the results of SCC tests of two candidate inner-container alloys exposed to an aqueous environment under the influence of applied electrochemical cathodic potential. The simulated conditions used in these tests are similar to an expected environment in the repository.

MATERIALS AND EXPERIMENTAL PROCEDURE

Materials tested include two titanium (Ti) – base alloys Ti Gr-7 (UNS R52400) and Ti Gr-12 (UNS R53400). The chemical compositions and room temperature mechanical properties of these alloys are given in Tables 1 and 2, respectively. The smooth tensile specimens (18.415-cm long and 1.109-cm nominal diameter with gage length and gage diameter of 2.54 cm and 0254 cm, respectively) were fabricated by a qualified vendor from the mill-annealed plate materials in the longitudinal rolling direction. No additional thermal treatments were given to these specimens prior to their testing.

The specimens were tested in a custom-made chamber made of polyvinylidene fluoride, and were vertically strained using an Instron testing machine. A strain rate of 3.3×10^{-6} sec^{-1} was used in all tests. The environment used for evaluating the susceptibility to SCC was a 90°C deaerated acidic brine (pH ≈ 2.7) containing 5 wt% NaCl. Acidification was done by adding 0.055 milliliter of reagent grade concentrated sulfuric acid (95-98%) per liter of salt solution. The selection of the acidic brine as test environment was based on the results of a recent SCC study[1,2] using the precracked wedge-loaded double-cantilever-beam specimens, which showed crack growth in Ti Gr-12 in a similar environment. Further, the acidified, concentrated brine was used to represent an extreme case in which microbiologically-influenced corrosion occurs as a result of microbial activity involving certain man-made materials (diesel fuels, organics, and sulfur-containing compounds) and water. These materials may be introduced into the repository during construction and operation, and may not be removed or may be inadvertently left behind when operations cease. The acidic pH can also simulate some of the effects of radiolysis.

Before being tested in the acidic brine, duplicate specimens of both alloys were pulled inside the test chamber in the dry condition at ambient temperature to establish a baseline. Additional specimens were then exposed to the 90°C acidic brine while being strained under different controlled electrochemical potentials (E_{cont}). The magnitude of E_{cont} was selected based on the stable open circuit or corrosion potential (E_{corr}) measured in the test solution before the specimens were strained. Silver/silver chloride (Ag/AgCl) reference electrodes were used in all SCC tests. Duplicate specimens of each material were tested under each experimental condition. The experimental setup is shown in Figure 1.

The load versus displacement curve for each specimen was recorded. The final gage diameter of the two halves of the broken tensile specimen were measured and used in computing the %RA. The maximum load before the test specimen failed was determined from the load versus displacement curve. σ_f was then calculated using this maximum load and the final cross sectional area at the gage section. The %El was determined from the original gage length and the displacement data. The TTF was calculated from the change in gage length, the original gage length and the strain rate used.

SIMS was used to analyze the hydrogen content of both alloys resulting from the cathodic charging. SEM and optical microscopy were used to characterize the cracking at the primary fracture face and along the gage section of the broken test specimen. Energy dispersive spectroscopic (EDS) analyses were performed on a few selected specimens to detect and identify chemical species present near the secondary cracking along the gage section of the tensile specimen. A section of the broken half showing the maximum damage was metallographically mounted and polished. A few selected specimens were also etched to determine the morphology of the cracking and verify the presence of hydrides in the vicinity of cracks.

RESULTS AND DISCUSSION

Cathodic (negative) potentials of 500, 1000 and 1200 mV with respect to the measured E_{corr} values (versus Ag/AgCl) were applied to the test specimens of both Ti Gr-7 and Ti Gr-12 as they were being pulled. In addition, Ti Gr-7 was potentiostatically polarized at a cathodic potential of 1500 mV with respect to the E_{corr} value while being strained at the same rate. For Ti Gr-7, the average E_{cont} values corresponding to these applied potentials were –675, -1122, -1329 and –1615 mV versus Ag/AgCl, respectively. The average controlled potentials for Ti Gr-12 were –465, -970 and –1162 mV versus Ag/AgCl, respectively. An attempt was made to evaluate the effect of these applied potentials on different ductility parameters. These E_{cont} values and the average E_{corr} values (versus Ag/AgCl) of the specimens tested without any externally applied potentials, were plotted as functions of σ_f, %RA, %El and TTF. The results indicate that the ductility of Ti Gr-12 in terms of both σ_f and %RA was gradually reduced with more cathodic applied potentials, as illustrated in Figures 2 and 3, respectively.

The effect of electrochemical potentiostatic polarization on %El and TTF for Ti Gr-12 are shown in Figures 4 and 5, respectively. It appears that %El and TTF were slightly increased with applied cathodic potentials of –465 and –970 mV followed by a reduction of both these parameters at an E_{cont} value of –1162 mV. Similarly, an evaluation of Figures 2 and 3 indicates that an application of –1162 mV to the Ti Gr-12 specimens produced the minimum values of σ_f and %RA. Figures 2 through 5 also illustrate the effect of E_{cont} on σ_f, %RA, %El and TTF, respectively for Ti Gr-7. Results (Figures 2 and 3) indicate that this material showed very little or no loss in ductility in terms of either σ_f or %RA as a function of applied cathodic potential. Further, no clear trend in these measured parameters was observed. As to the effect of E_{cont} on %El and TTF, the results shown in Figures 4 and 5, respectively indicate that there was a gradual increment in both these parameters with applied potentials up to –1000 mV with respect to the measured E_{corr} values. However, at more cathodic applied potentials, somewhat lower values were observed.

The basic difference in chemical composition between the tested alloys, as shown in Table 1, is that the Ti Gr-7 contains palladium (Pd) while Ti Gr-12 is alloyed with molybdenum (Mo) and nickel (Ni). Ti Gr-7 consists of a single α-phase having hexagonal close-packed crystal structure. On the other hand, Ti Gr-12 is a near-α alloy containing relatively small amount of β-phase with body-centered cubic crystal structure in an α matrix. The effect of controlled potential on the ductility parameters, as observed in this study, may be interpreted in terms of the partitioning of hydrogen generated during cathodic charging between the α and β phases, and the effect of hydrogen on the lattice parameters of these two phases.

There are indications in the literature[3,4] that Ti and its alloys can absorb hydrogen when they are charged at cathodic potential or when they are galvanically coupled to more active metals and alloys, thus becoming cathodes. Hydrides can be formed in Ti alloys when the hydrogen absorption reaches a critical level. These acicular hydride platelets, which are known to be brittle, can adversely influence the physical properties including ductility parameters evaluated in this study. The detrimental effect of cathodic applied potentials in enhancing the hydrogen-induced embrittlement or hydrogen embrittlement (HE) of Ti Gr-3 (an α-type Ti alloy) in a 70°C acidic brine (6 wt% NaCl) has been reported by Wang et al.[5] The formation of thicker hydride layers at more cathodic applied potentials has been attributed to the increased susceptibility of this alloy to HE in their study. The effect of hydrogen charging on the mechanical behavior of Ti-6Al-4V (an α-β type Ti alloy) has been investigated by Gu and Hardie.[6] These investigators showed that the ductility of this alloy was drastically reduced when the hydrogen content exceeded a critical value of 2000 ppm. Their results suggest that this alloy may undergo HE at such a hydrogen level.

The susceptibility to hydrogen-induced cracking of Ti grades 2 and 12 has been studied by Azkarate et al[7] in synthetic seawater at ambient temperature using the SSR technique. Their results showed that Ti Gr-2 did not suffer from ductility loss due to cathodic charging. However, at an applied potential of –1500 mV, a few small secondary cracks were observed and superficial hydrides were detected. For Ti Gr-12, the cracking susceptibility in their study was more pronounced with a significant reduction in ductility, in particular, in %RA and σ_f. Considerable hydrides were detected in the bulk material and numerous brittle secondary cracks were noticed along the gage section of the test specimens potentiostatically polarized at –1500 mV.

Figure 6 illustrates the effect of controlled electrochemical potential on the absorbed hydrogen concentration analyzed by SIMS at different locations (close to the primary fracture) of the gage section of the specimens tested either in air or in the acidic brine. These data indicate that the concentration of hydrogen in both Ti Gr-7 and Ti Gr-12 was increased with more cathodic applied potential. These results may also suggest that the amount of hydrogen generated in these alloys as a result of potentiostatic polarization at comparable cathodic potentials was not significantly influenced by their chemical

compositions. Further, the concentrations of hydrogen generated in these alloys at different E_{cont} values are significantly lower than the critical hydrogen content of 2000 ppm, reported by Gu and Hardie (1996)[6] for HE to occur in Ti-6Al-4V.

The results of the metallographic evaluation of broken test specimens by optical microscopy indicate that both materials became susceptible to secondary cracking along the gage section while being strained in the aqueous environment, regardless of the magnitude of the E_{cont} values (Figures 7 and 8). However, in general, the extent of cracking was more pronounced in Ti Gr-7, showing multiple cracks, as illustrated in Figure 9. It appears that the cracking was transgranular in both alloys. An effort was made to correlate the deepest secondary crack length to the E_{cont} value. However, no systematic correlation could be made from this analysis.

The morphology of primary and secondary cracking of both alloys was further analyzed by SEM. The results, shown in Figures 10 and 11, indicate that regardless of the E_{cont} values the cracking at the primary fracture face was ductile, showing dimpled microstructures. On the contrary, SEM micrographs taken along the gage section of the test specimens revealed transgranular brittle or quasi-cleavage failures as illustrated in Figures 12 and 13. Analyses of EDS spectra at the tip and edge of the crack, and at the matrix of the Ti Gr-7 specimen tested at an E_{cont} values of –1592 mV, revealed the presence of titanium alone (Figure 14).

Initiation of SCC in titanium alloys in aqueous environments has been attributed[8,9] to planar slip and the formation of wide slip steps that rupture the protective surface-oxide (TiO_2) films. Unless rapid repassivation of these surface films occurs, an active trench may be formed due to the localized anodic dissolution at the metal surface. This active trench, if sufficiently localized, can eventually cause the stress corrosion crack growth.

Two theories have been proposed[8,9] to account for SCC propagation of Ti alloys in susceptible aqueous environments. One theory[8,9] is based on anodic dissolution of metal surface at highly localized areas of stress concentration such as the crack tip, which can aid in crack propagation into the metal by the applied tensile stress. The other prominent mechanism[8,9] is centered on the HE phenomenon that may possibly account for the cracking of Ti alloys studied in this investigation. This mechanism postulates that hydrogen absorption can result from localized anodic dissolution in a hydrogen-containing aqueous solution, and the formation of film-free surfaces within the advancing crack. Absorbed hydrogen may then migrate and concentrate near the crack tip due to the existing tensile stress gradients. Localized HE of the metal ahead of the crack tip can subsequently aid in continued crack growth. This mechanism has been cited[8,9] to be prominent for α- and α/β-types of Ti alloys, where localized precipitation of brittle titanium hydrides ahead of the advancing crack could promote transgranular brittle failure.

It is well known that excessive hydrogen uptake due to cathodic charging can induce the precipitation of hydrides in Ti alloys. Hydrogen pick-up is dependent on both the solubility and diffusivity of hydrogen. The three conditions that must be met for HE to occur are: the generation of critical concentration of atomic hydrogen on the alloy surface resulting from the application of cathodic potential, the exposure at temperatures at which the diffusion rate of hydrogen is significant, and the maintenance of solution pH at or below 3. A temperature of 80°C has been cited[10] to be the critical temperature above which hydrogen diffusion through the titanium surface oxide film may be significant. Since cracking was observed in both alloys in the same environment under cathodic applied potentials, an effort was made to characterize the hydrides formed in Ti Gr-7 by both optical microscopy and SEM. Lath-like appearance of hydrides, as detected by SEM, is shown in Figure 15 for Ti Gr-7 potentiostatically polarized at an E_{cont} value of –1638 mV versus Ag/AgCl.

SUMMARY AND CONCLUSIONS

Smooth tensile specimens were tested to evaluate the SCC susceptibility of Ti Gr-7 and Ti Gr-12 in a 90°C deaerated acidic brine, with and without impressed cathodic potential at a strain rate of 3.3×10^{-6} sec^{-1}. A few tests were also performed inside the test chamber in the dry condition at ambient temperature. The ductility parameters were evaluated as a function of the applied electrochemical potential. The morphology of the primary and secondary cracking in the test specimens was characterized by both optical microscopy and SEM. Hydrogen concentration along the gage length of the test specimen was analyzed by SIMS. EDS analyses were performed on a few selected specimens. The significant conclusions drawn from this study are summarized below.

- The ductility of Ti Gr-12 in terms of σ_f and %RA was gradually reduced with more cathodic E_{cont} values. A slight increase in %El and TTF was observed at E_{cont} values of –465 and –970 mV (Ag/AgCl) followed by their reduction at –1162 mV (Ag/AgCl).

- Very little or no loss of ductility in terms of either σ_f or %RA as a function of E_{cont} was observed with Ti Gr-7. Slight gradual increment in %El and TTF was noticed with applied potentials of up to −1000 mV with respect to the E_{corr} values. Reduced values of these two parameters were obtained at more cathodic potentials.

- In general, the concentration of hydrogen in both alloys analyzed by SIMS was increased with more cathodic applied potential.

- Both alloys showed secondary cracking along the gage section of the test specimen regardless of the magnitude of the E_{cont} value. However, cracking was more severe in Ti Gr-7. The secondary cracks in both alloys were transgranular (brittle or quasi-cleavage), confirming observations by other investigators. The primary fracture face was characterized by dimpled microstructure, typical of ductile failure.

- Acicular hydrides were detected suggesting that the initiation and growth of cracking in titanium alloys may be the result of hydrogen absorption due to cathodic charging and localized precipitation of brittle titanium hydrides ahead of the advancing crack, thus promoting transgranular brittle failure.

ACKNOWLEDGMENTS

This work was performed under the auspices of the U.S. Department of Energy under contract number W-7405-ENG-48 at the Lawrence Livermore National Laboratory. The support of the Yucca Mountain Site Characterization Project is thankfully acknowledged.

Acknowledgment is also made to Robert Kershaw and Edward Sedillo for their sincere help in metallography and SEM-EDS study, respectively. Finally, thanks and appreciation are extended to Anthony Sanchez for his expert assistance in TID work.

REFERENCES

1. A. K. Roy, D. L. Fleming, D. C. Freeman and B. Y. Lum, "Stress Corrosion Cracking of Alloy C-22 and Ti Gr-12 using Double-Cantilever-Beam Technique," Micron Vol. 30, No. 6, pp. 647-652, 1999.

2. A. K. Roy, D. L. Fleming and B. Y. Lum, "Stress Corrosion Cracking of Fe-Ni-Cr-Mo, Ni-Cr-Mo and Ti Alloys in a 90°C Acidic Brine," NACE Corrosion/98, Paper No. 157, San Diego, CA, March 22-27, 1998.

3. R. W. Schutz and J. S. Grauman, "Determination of Cathodic Potential Limits for Prevention of Titanium Tube Hydride Embrittlement in Salt Water," NACE Corrosion/89, Paper No. 110, New Orleans, LA, April 17-21, 1989.

4. H. Satoh, T. Fukuzuka, K. Shimogori and H. Tanabe, "Hydrogen Pickup by Titanium Held Cathodic in Seawater," 2nd Int. Cong. Hydrogen in Metals, Paper No. 6A1, Paris, France, June 6-11, 1977.

5. Z. F. Wang, C. L. Briant and K. S. Kumar, "Hydrogen Embrittlement of Grade 2 and Grade 3 Titanium in 6% Sodium Chloride Solution," Corrosion Vol. 54, No. 7, pp. 553-560, 1998.

6. J. Gu and D. Hardie, "Effect of Hydrogen on Structure and Slow Strain Rate Embrittlement of Mill Annealed Ti6Al4V," Materials Science and Technology (UK) Vol. 12, No. 10, pp. 802-807, 1996.

7. I. Azkarate, A. Pelayo and L. Victori, "Hydrogen Assisted Stress Cracking of Titanium Alloys in Aqueous Chloride Environments," Progress in the Understanding and Prevention of Corrosion Vol. II, Barcelona, Spain, pp. 1573-1580, 1993.

8. R.J.H. Wanhill, "Aqueous Stress Corrosion in Titanium Alloys," Br. Corros. J. Vol. 10, No. 2, pp. 69-78, 1975.

9. J. Brettle, "Stress Corrosion of Titanium and Its Alloys in Aqueous Chloride Environments," Met. Mater., pp. 442-451, October 1972.

10. L. C. Covington, "The Influence of Surface Condition and Environment on the Hydriding of Titanium," Corrosion Vol. 35, No. 8, PP. 378-382, August 1979.

TABLE 1
CHEMICAL COMPOSITION OF MATERIALS TESTED (WT%)

Material	Lot #	C	Ni	Mo	Fe	Pd	Ti	O	N	H
UNS R52400	P246	0.012	---	---	0.08	0.15	Bal	0.14	0.007	<0.002
UNS R53400	N242	0.007	0.93	0.31	0.18	---	Bal	0.12	0.008	0.0051

TABLE 2
ROOM TEMPERATURE MECHANICAL PROPERTIES

Material	Lot #	YS (MPa)	UTS (MPa)	%El	%RA	Hardness
Ti Gr-7	P246	385.4	509.7	25.3	NA	NA
Ti Gr-12	N242	392.3	560.4	18	NA	NA

NA: Not Available

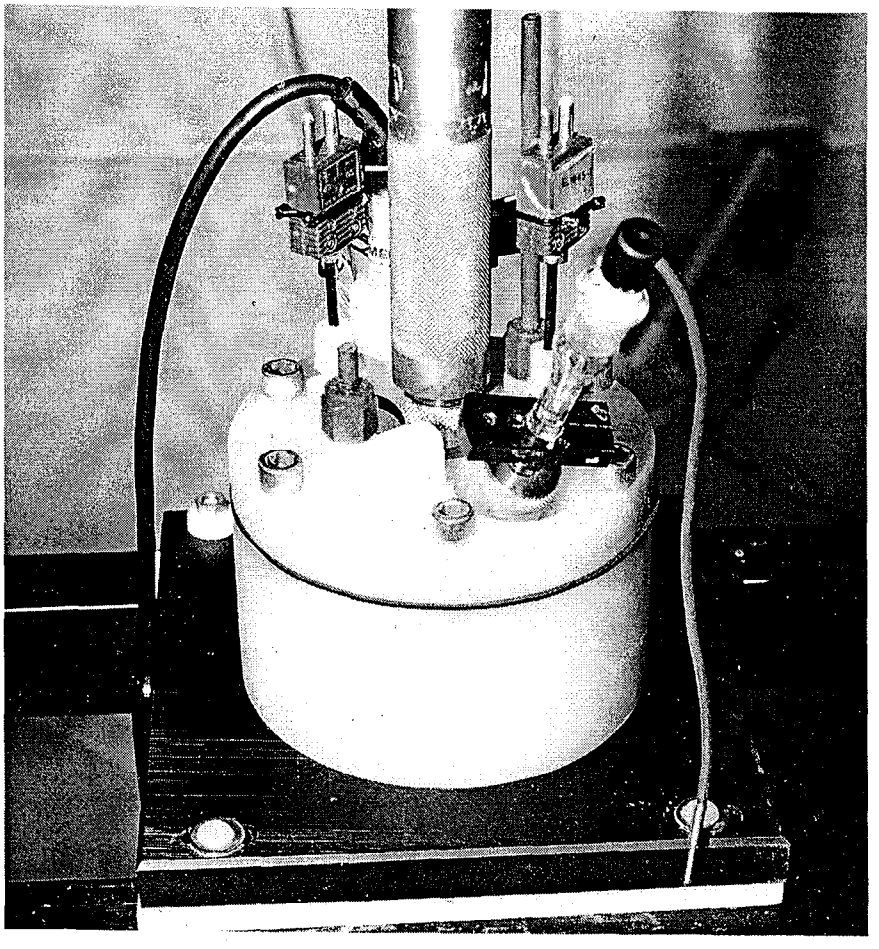

Figure 1. Test Setup

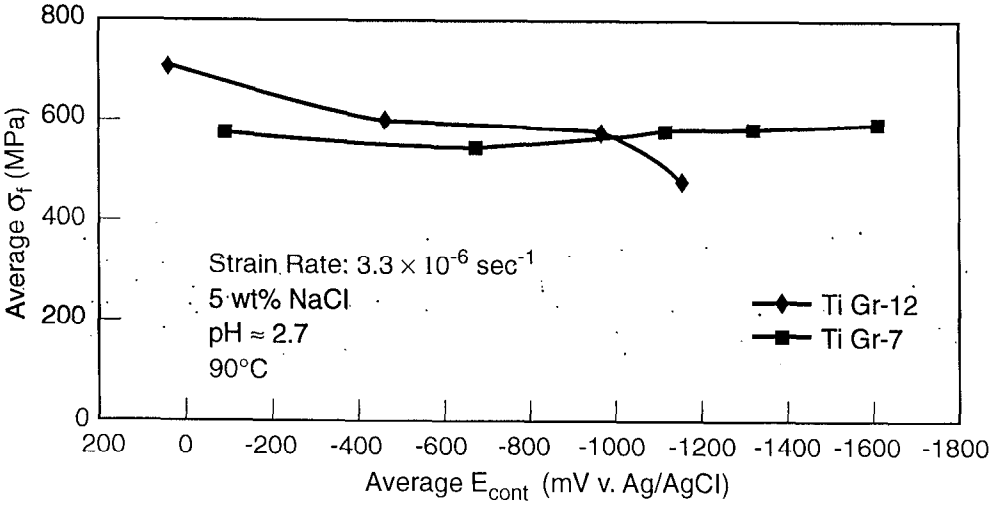

Figure 2. σ_f versus E_{cont}

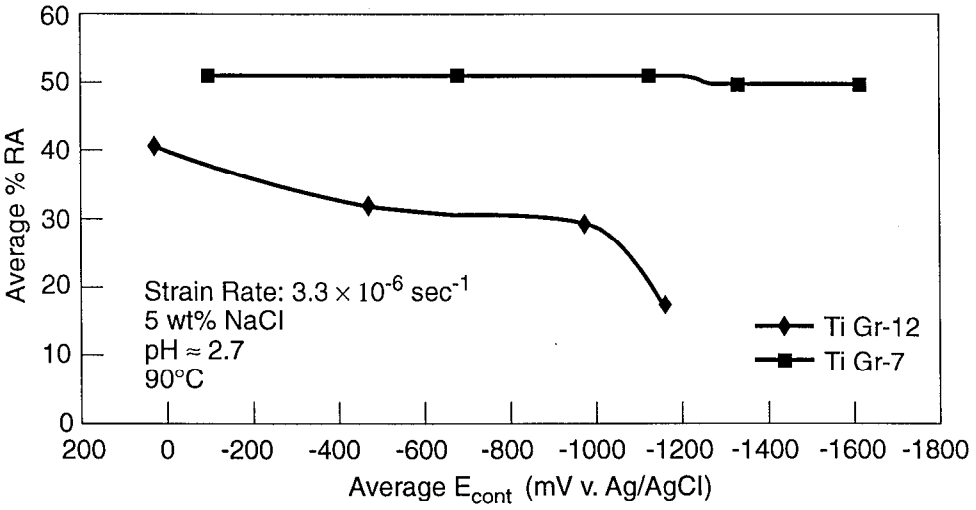

Figure 3. % RA versus E_{cont}

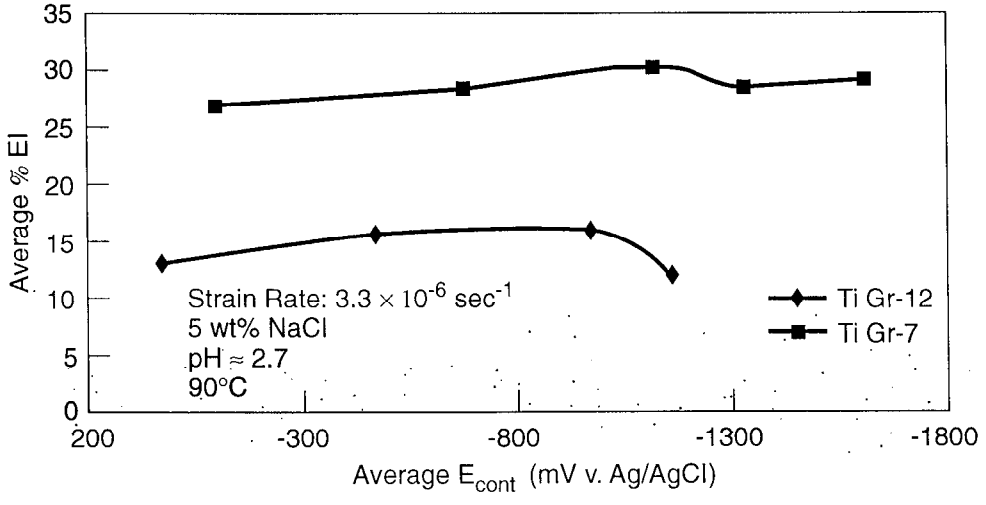

Figure 4. % EI versus E_{cont}

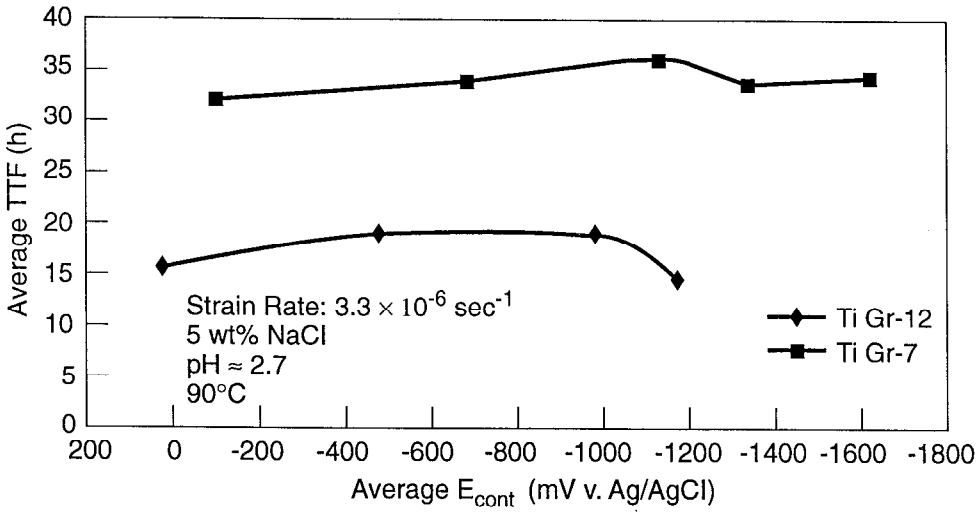

Figure 5. TTF versus E_{cont}

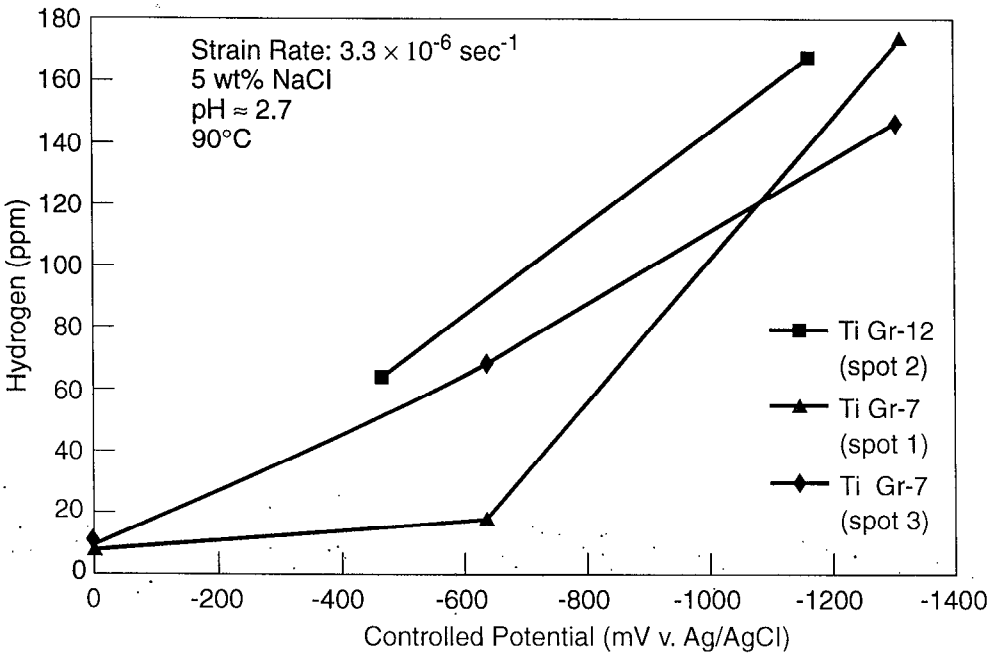

Figure 6. Hydrogen Concentration versus E_{cont} at Locations away from the Primary Fracture.

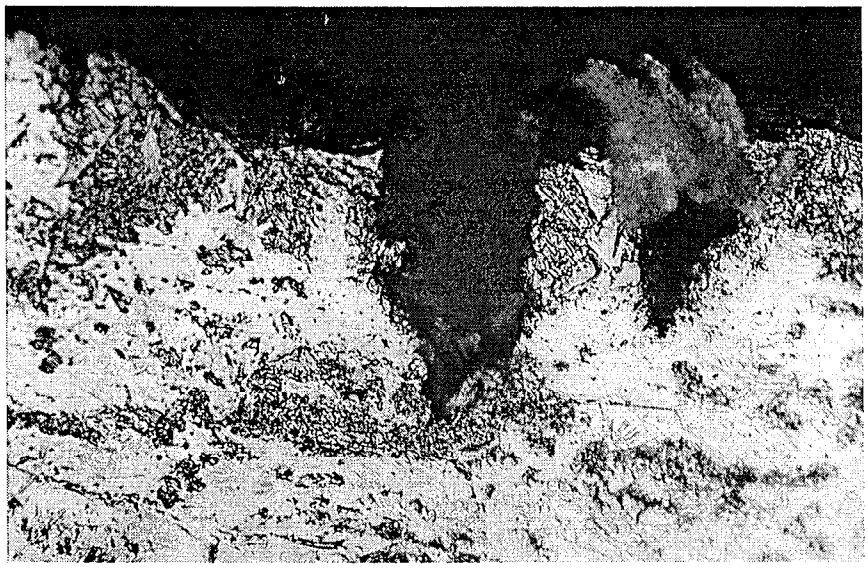

Figure 7. Secondary Cracking of Ti Gr-7 at an E_{cont} Value of –715 mV (Ag/AgCl). Etchant: 3% HF + 6% HNO_3 + Water. 500X

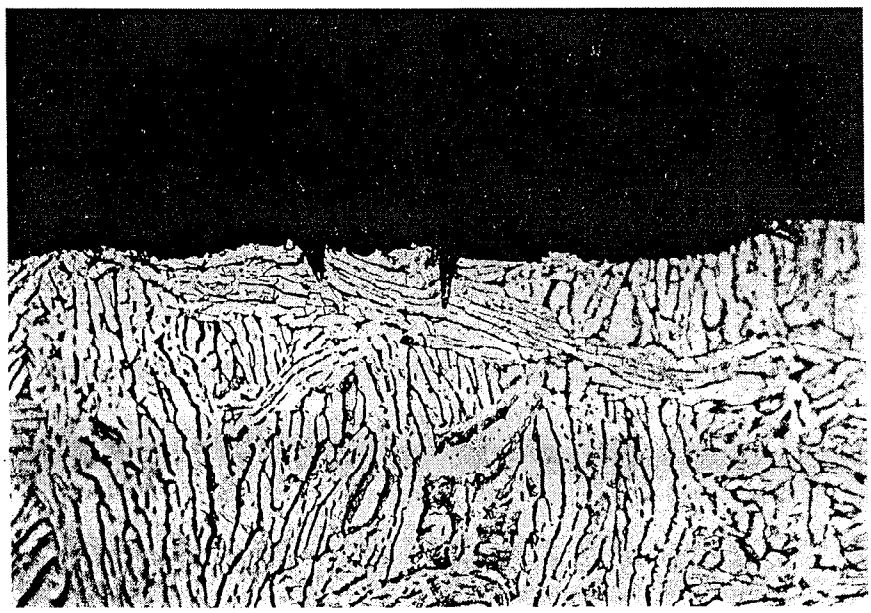

Figure 8. Secondary Cracking of Ti Gr-12 at an E_{cont} Value of –465 mV (Ag/AgCl). Etchant: 3% HF + 6% HNO_3 + Water. 500X

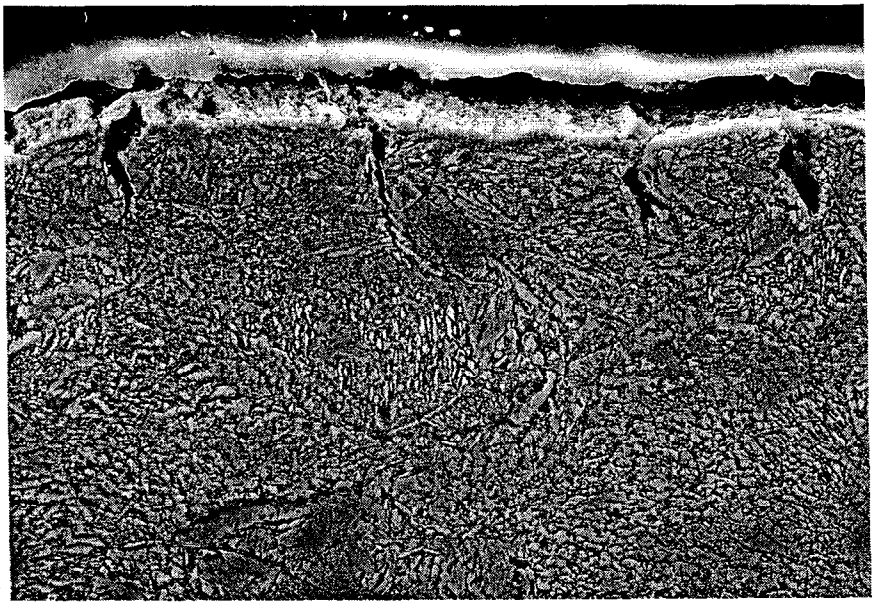

Figure 9. SEM Micrograph Showing Multiple Secondary Cracks in Ti Gr-7 at an E_{cont} Value of –1592 mV (Ag/AgCl). Etchant: 3% HF + 6% HNO_3 + Water. 1000X

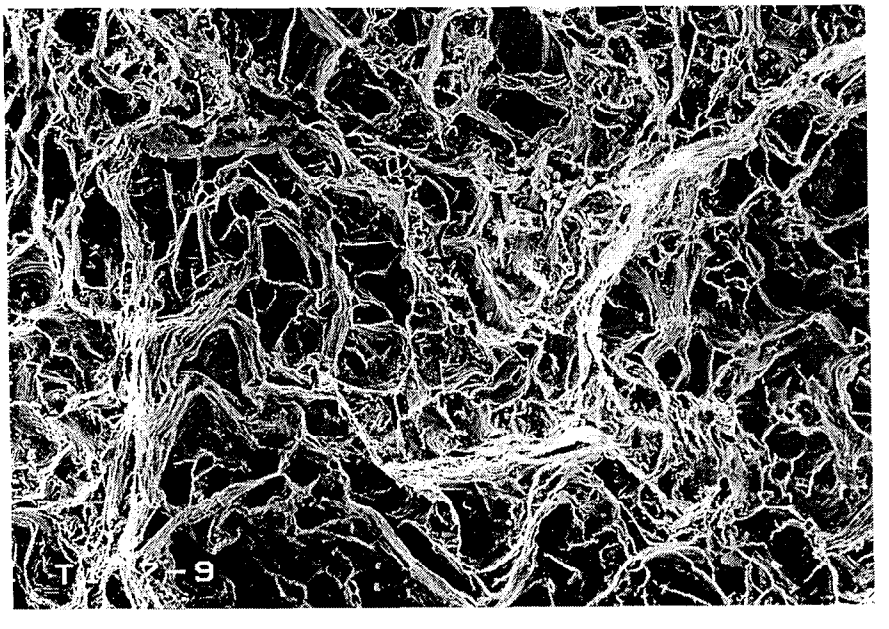

Figure 10. SEM Micrograph Showing Dimpled Microstructure of Ti Gr-7 at the Primary Fracture Face at an E_{cont} Value of –1305 mV (Ag/AgCl). 250X

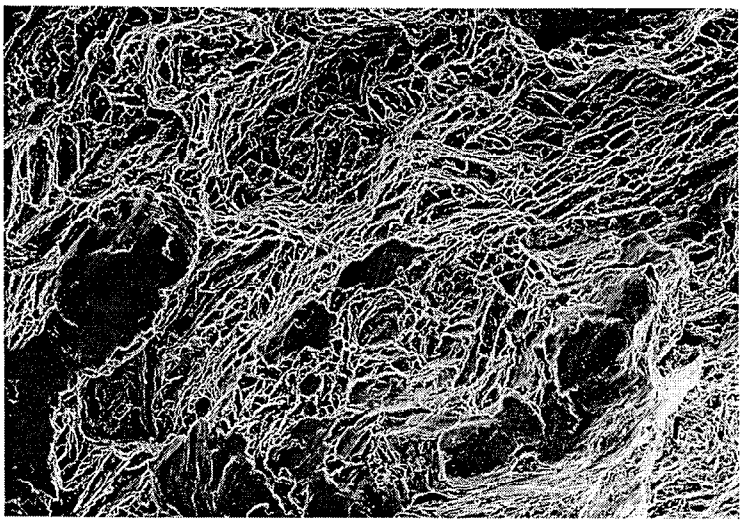

Figure 11. SEM Micrograph Showing Dimpled Microstructure of Ti Gr-12 at the Primary Fracture Face at an E_{cont} Value of –1136 mV (Ag/AgCl). 250X

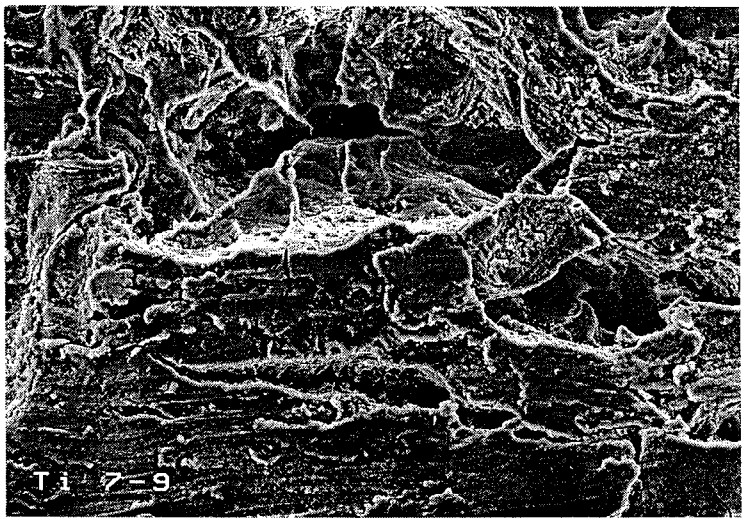

Figure 12. SEM Micrograph Showing Transgranular Secondary Brittle Failure of Ti Gr-7 at an E_{cont} Value of –1305 mV (Ag/AgCl). 500X

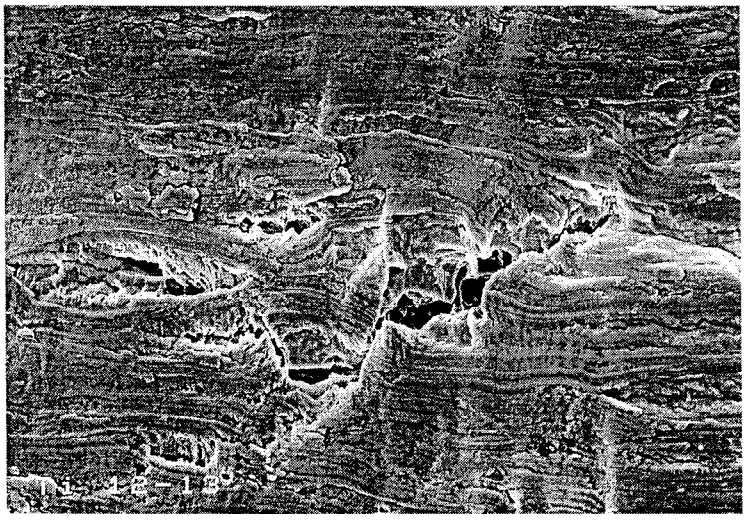

Figure 13. SEM Micrograph Showing Transgranular Secondary Brittle Failure of Ti Gr-12 at an E_{cont} Value of –1136 mV (Ag/AgCl). 500X

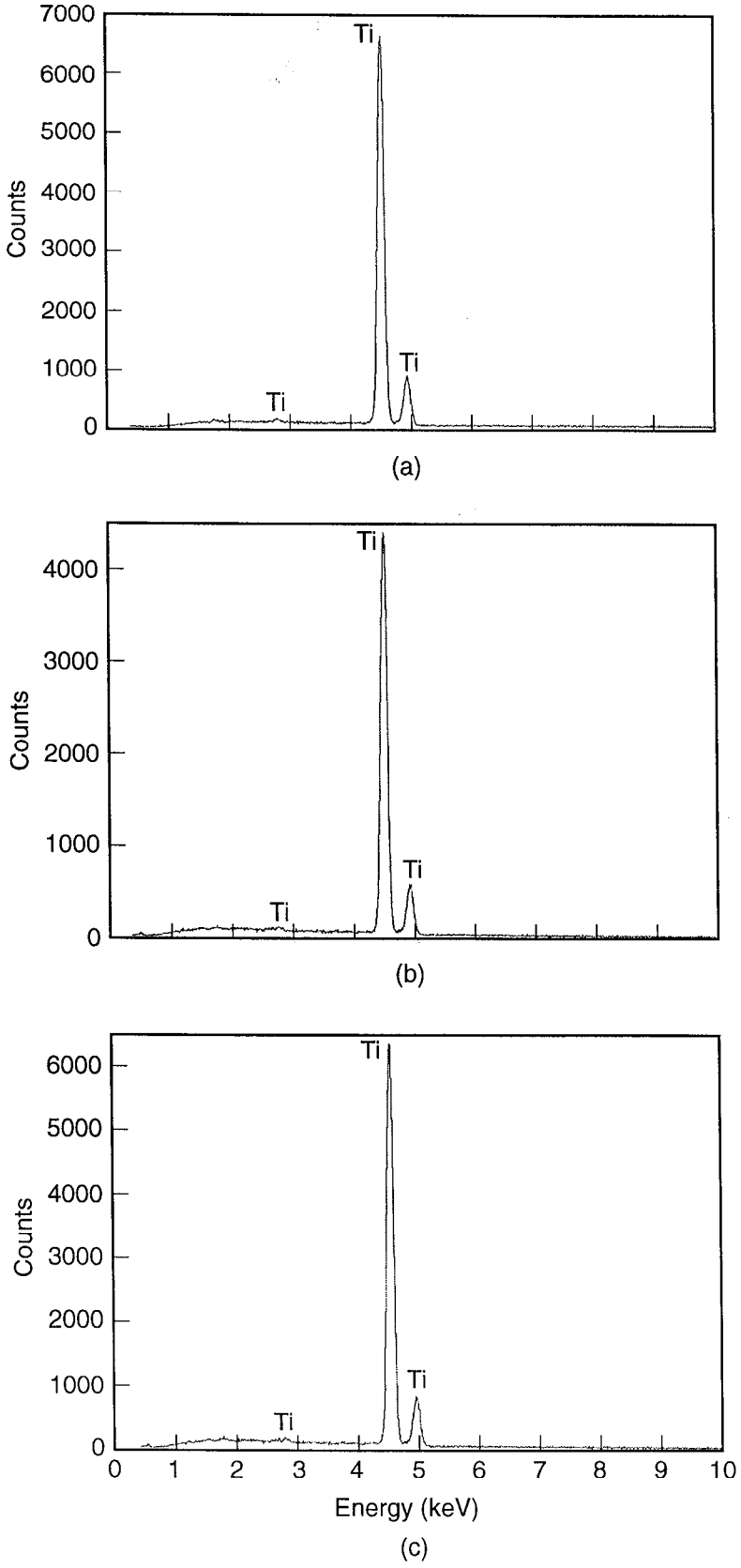

Figure 14. EDS Spectra for Ti Gr-7 at three locations.
(a) Crack Tip (b) Crack Edge (c) Matrix.

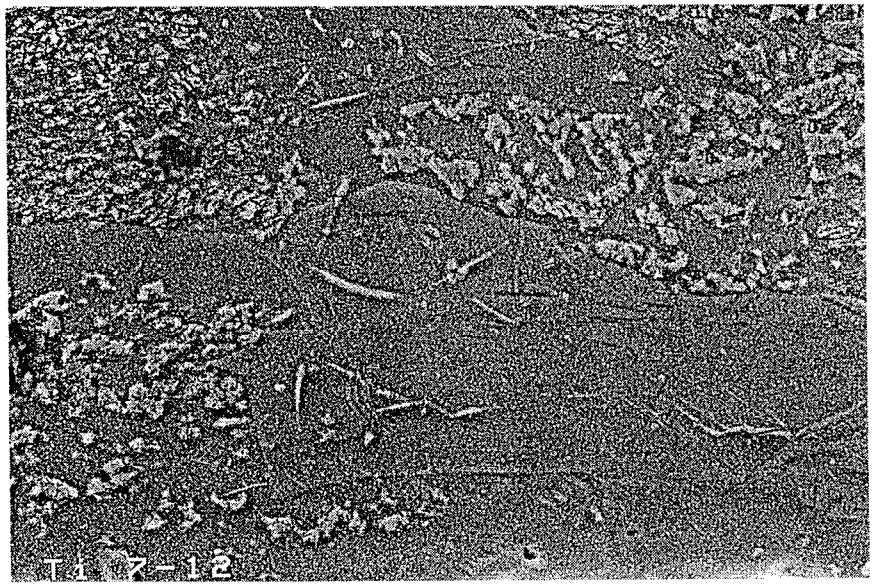

Figure 15. SEM Micrograph Showing Hydrides in Ti Gr-7 at an E_{cont} Value of –1638 mV. 1000X